Hindawi Publishing Corporation
International Journal of Distributed Sensor Networks
Volume 2013, Article ID 281895, 8 pages
http://dx.doi.org/10.1155/2013/281895

Research Article

Tone-Independent Orthogonalizing Lattice Equalization for Insufficient Cyclic-Prefix OFDM Transmissions

Dong Kyoo Kim[1] and Yang Sun Lee[2]

[1] *Electronics and Telecommunications Research Institute, Daejeon 305-700, Republic of Korea*
[2] *Division of Computer Engineering, Mokwon University, Daejeon 302-729, Republic of Korea*

Correspondence should be addressed to Yang Sun Lee; yslee48@gmail.com

Received 24 September 2013; Revised 1 November 2013; Accepted 4 November 2013

Academic Editor: Jongsung Kim

Tone-independent orthogonalizing lattice per tone equalizer (TOL-PTEQ) is introduced and its convergence is analyzed. Cyclic-prefix redundancy, one of the major drawbacks of orthogonal frequency division multiplexing (OFDM), can be reduced by TOL-PTEQ. Fast convergence and low computational complexity of TOL-PTEQ are also suitable properties for packet-based wireless communications and detections in which OFDM is widely deployed for their modulation technique.

1. Introduction

PTEQ was originally proposed for optimizing bit rate of discrete-multitone (DMT) modem in wired communications such as digital subscriber lines (DSLs), where SNR of each tone can be independently maximized [1–4]. In these literatures, computational complexity is a major issue because they should cover a large number of tones, for example, DMTs with 512, 1024, or 2048 tones. Several types of stochastic-gradient algorithms for PTEQ have been proposed to reduce the computational complexity [1, 2]. But convergence rate is considered as a minor issue for DSLs because various DSLs have long training sequences in their initial set-up process.

Wireless broadband communication technology is becoming more important for pervasive healthcare solutions as healthcare applications [5–7] are extending their coverage up to global scale as shown in Figure 1 [8]. According to [8], researches on more fast and reliable wireless infrastructures are conducted in order to improve the healthcare services in remote location. Candidate wireless technologies are as follows: IEEE 802.11x, IEEE 802.16x, ETSI HiperLAN, ETSI HiperMAN, and so on. A common feature of the candidates is that they use OFDM as their modulation method which is the promising technology because it is easy to handle the multipath channel problem by using fast Fourier transform. It is also widely utilized for multiple-access method, say OFDMA. It gives multiuser diversity taking advantage of channel frequency selectivity and good scalability over wide range of bandwidth that is achieved just by adjusting FFT size, where FFT stands for fast Fourier transform [9]. OFDM can also be utilized in the field of radar technologies as shown in Figure 2, where the multitone technique can be applied to enhance the radar scanning performance [10]. In this case, various OFDM technologies are essential to the multitone based radar systems. As shown in Figure 2, the radar transmits and receives the radar signal through the antennas. The received signal contains various reflection signals generated by the interfaces between two different layers. To obtain the high-resolution reflection signals, the radar system should use the ultrawideband signal, which can be created by composing several narrowband signals as shown in Figure 2. The multitone based radar system uses the multitone signal as the narrowband signal, in which we can utilize various existing advanced technologies of OFDM such as the channel estimation and the computationally efficient and fast implementation architectures.

Two major drawbacks of OFDM are the peak-to-average power ratio and cyclic-prefix (CP) redundancy. To cope with the CP redundancy problem that decreases spectral efficiency, several approaches have been proposed [11, 12]. In [11], iterative cancellation method was used to cancel interferences due to the insufficient CP, where terrestrial HDTV

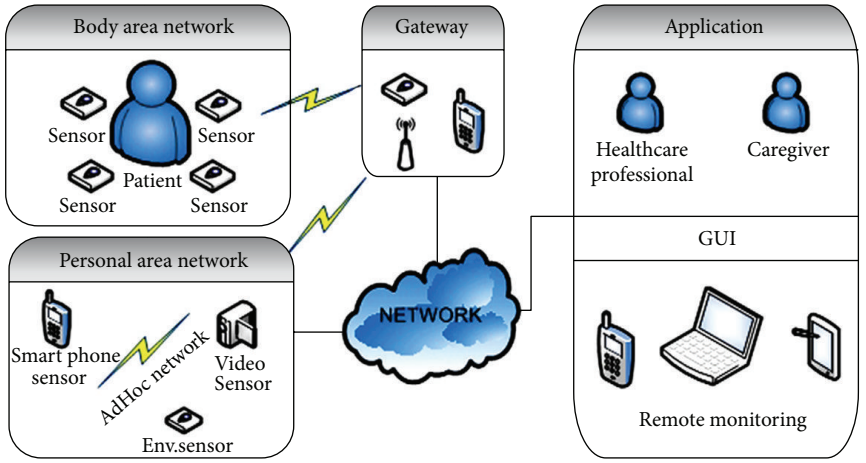

Figure 1: Overview of a simple WSN application scenario for healthcare (this figure is quoted from Figure 1 in [8]).

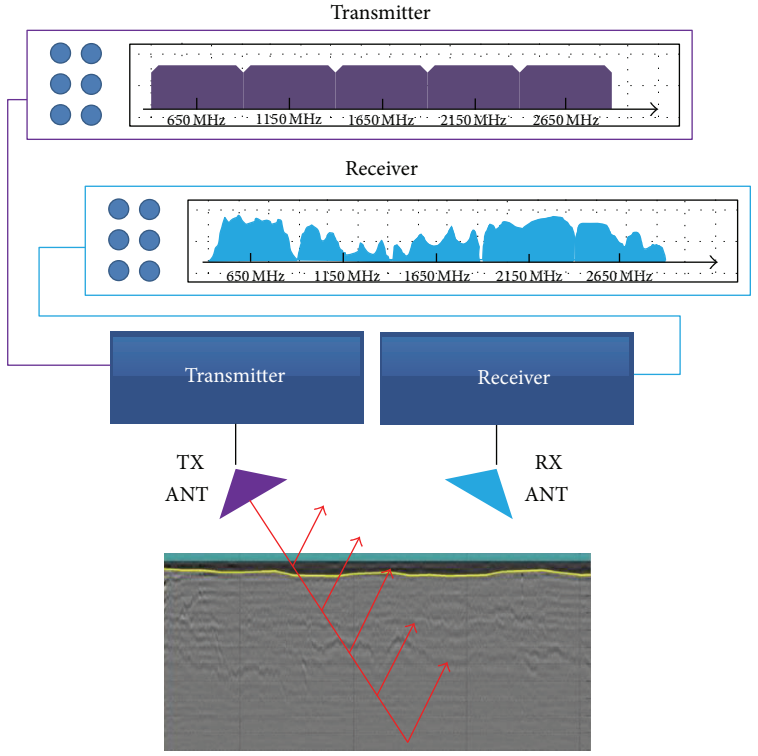

Figure 2: Multitone based radar technology.

broadcasting scenario was considered as its application. As mentioned in page 1598 of [11], computational burdens of iterations are very big because $2I + 2$ FFT operations are needed for I iterations. In [12], precompensation was used to avoid differential group delay of optical OFDM systems. This precompensation of delay can ensure zero intersymbol interference while reducing CP length. To do this, channel state information is fed back from receiver to transmitter.

PTEQ technique can be applied to the CP reduction problem of the OFDM-based wireless communication systems because PTEQ is the frequency-domain version of the time-domain channel-shortening equalizer (TEQ) which shortens channel impulse response length [13, 14]. Thus, this shortening property can be applied to the problem that makes CP length less than the channel impulse response length. Almost all wireless OFDM systems are based on packet-based

transmissions and a quasistatic environment is assumed, where a packet consists of a preamble and a payload. A new channel estimation should be performed in every packet; thus fast convergence of PTEQ is needed not to slow down the overall transmission throughput.

In this paper, we analyze convergence properties of the existing PTEQ algorithms. It will be shown that their convergence properties are related to eigenvalue spread of PTEQ-input signals especially in the initial training period.

We then show a stochastic-gradient lattice-typed PTEQ algorithm, TOL-PTEQ, with fast convergence rate while maintaining a low computational complexity, where its convergence rate is fast enough for packet-based wireless communications. As opposed to the existing transversal filter-based PTEQs, TOL-PTEQ has lattice feature to orthogonalize a portion of its input signals with low computational complexity. To the best of our knowledge, there is no approach in which the lattice-typed PTEQ is applied to the OFDM technology before. We also provide the convergence model of TOL-PTEQ, where the accuracy of the model is shown by comparing the model with numerical simulation results.

The rest of this paper is organized as follows. In Section 2, problem setup for PTEQ is described and one existing PTEQ algorithm, RLSLMS-PTEQ, is analyzed. In Section 3, TOL-PTEQ is shown in detail. In Section 4, simulation results and comparisons of the various PTEQ algorithms are provided. Finally, conclusion is provided in Section 5.

2. Problem Setup and RLSLMS-PTEQ

2.1. Problem Setup. Signal vector $\mathbf{x}^{(k)}$ at block time k is transmitted and propagated through the $(L+k+1)$th-order channel $\mathbf{h}$. Then, the received signal vector $\mathbf{y}^{(k)}$ is written as

$$\mathbf{y}^{(k)} = \left[\mathbf{O} \mid \mathrm{T}\left(\left[h_L \;\; \mathbf{0}_{1X(L+K)}\right]^T, \left[\mathbf{h} \;\; \mathbf{0}_{1X(L+K)}\right]\right) \mid \mathbf{O}\right] \cdot \mathbf{x}^{(k)} + \mathbf{n}^{(k)}, \tag{1}$$

where the superscript T is the transpose operator, $\mathrm{T}(\mathbf{a}, \mathbf{b})$ is the Toeplitz matrix of which first column and row vector are $\mathbf{a}$ and $\mathbf{b}$, L and K are the length of post- and precursors, and $\mathbf{n}^{(k)}$ is the white Gaussian noise vector.

According to [1], (1) is equalized by the Tth-order PTEQ $\overline{\mathbf{v}}_i$ of the ith subcarrier and its output can be written as

$$Z_i^{(k)} = \overline{\mathbf{v}}_i^T \begin{bmatrix} \mathbf{I}_{T-1} & \mathbf{O}_{(T-1)X(N-T-1)} & -\mathbf{I}_{T-1} \\ \mathbf{0}_{1X(T-1)} & F_N(i,:) & \end{bmatrix} \mathbf{y}^{(k)} = \overline{\mathbf{v}}_i^T \mathbf{u}^{(k)}, \tag{2}$$

where $F_N(i,:)$ is the ith row vector of N-point FFT matrix, $\mathbf{u}^{(k)} = \left[\mathbf{d}^{(k)T} \;\; Y_i^{(k)}\right]$ is the input vector, $Y_i^{(k)}$ is the Fourier transform of $\mathbf{y}^{(k)}$, and $\mathbf{d}^{(k)} \equiv \left[d_0^{(k)} \;\; \cdots \;\; d_{T-2}^{(k)}\right]$ is the difference vector of which element is written as $d_l^{(k)} \equiv -y_{(k+1)s-l} + y_{ks+\nu-l}$. $\widehat{\overline{\mathbf{v}}}_i^{\mathrm{opt}}$ is hereby the estimated optimal vector that minimizes the expectation of $|Z_i^{(k)} - X_i^{(k)}|^2$, where $X_i^{(k)}$ is the training or pilot subcarrier signal.

The most powerful algorithm to obtain $\widehat{\overline{\mathbf{v}}}_i^{\mathrm{opt}}$ is the recursive least squares (RLS). The performance of RLS-PTEQ [15] will be shown in Section 3, in which it outperforms other PTEQs. In case that the number of subcarriers is large, stochastic-gradient-based algorithms such as NLMS-PTEQ and RLSLMS-PTEQ [2] are preferred because the computational complexity of RLS-PTEQ is too big to be implemented. However, convergence rates of the stochastic-gradient-based PTEQs are so slow that they may slow down the transmission throughput of packet-based wireless communications. The convergence of these stochastic-gradient PTEQs is highly related to the eigenvalue spread of their input autocorrelation matrix $R_{\mathbf{uu}} = E[\mathbf{u}^{(k)}\mathbf{u}^{(k)H}]$, where superscript H denotes the Hermitian. $\mathbf{u}^{(k)}$ is highly correlated because its elements consist of the combination of received signals. With high eigenvalue spread, it is well known that NLMS-PTEQ has poor performance in the sense of convergence rate and steady-state misadjustment; this can be also seen through simulations in Section 3.

RLSLMS-PTEQ which combines NLMS-PTEQ with RLS-PTEQ has effectively low computational complexity compared with that of RLS-PTEQ, where RLS is not used for $\overline{\mathbf{v}}_i$ update but for only $\mathbf{d}^{(k)}$ calculations. Main purpose of RLSLMS-PTEQ is the decorrelation of $\mathbf{d}^{(k)}$ with computationally complex RLS, and this decorrelation result is commonly utilized to all subcarriers' PTEQ in which the equalization of each subcarrier is performed by simple NLMS. The steady-state misadjustment of RLSLMS-PTEQ is close to that of RLS-PTEQ. However, its convergence rate is much slower than that of RLS-PTEQ as shown in [2], and it will be further discussed in the next section.

2.2. Analysis of RLSLMS-PTEQ. The autocorrelation $R_{\mathbf{lu}}$ of RLSLMS-PTEQ has, approximately, $(T-2)$ eigenvalues of $1/W$ and two eigenvalues of $(1 \pm d)/W$ with d as

$$d = \sqrt{\frac{W^2}{e_i^{(k+1)}} E\left[Y_i^* \mathbf{d}^{(k+1)T}\right] \overline{\mathbf{S}}^{(k+1)T} \overline{\mathbf{S}}^{(k+1)} E\left[\mathbf{d}^{(k+1)} Y_i\right]}, \tag{3}$$

where d, W, $\mathbf{l}$, $\overline{\mathbf{S}}_i$, and $e^{(k+1)}$ are defined in [2]. Equation (3) can be written as

$$\begin{aligned} d &= \sqrt{\frac{W^2}{e_i^{(k+1)}} E\left[Y_i^* \mathbf{d}^{(k+1)T}\right] E\left[\overline{\mathbf{k}}^{(k+1)} Y_i\right]} \\ &= \sqrt{\frac{W^2}{e_i^{(k+1)}} E\left[Y_i^* Y_i \mathbf{d}^{(k+1)T} \overline{\mathbf{k}}^{(k+1)}\right]} \\ &\approx \sqrt{WE\left[\mathbf{d}^{(k+1)T} \overline{\mathbf{k}}^{(k+1)}\right]}, \end{aligned} \tag{4}$$

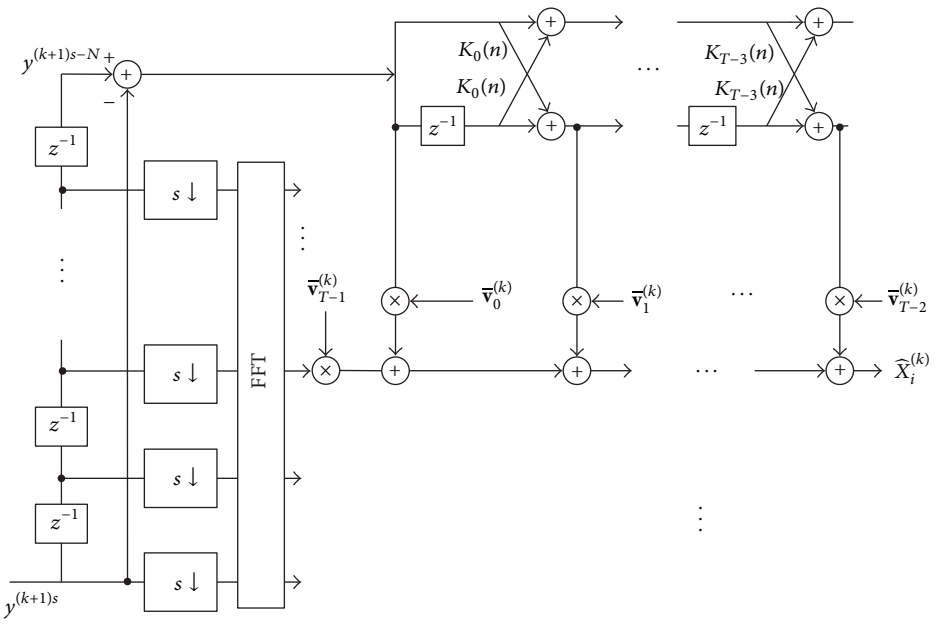

Figure 3: Structure of TOL-PTEQ.

where $\overline{\mathbf{k}}^{(k+1)} = \overline{\mathbf{S}}^T \overline{\mathbf{S}} \mathbf{d}^{(k+1)}$. Conversion factor is defined as

$$\overline{\gamma}^{(k+1)} = 1 - \mathbf{d}^{(k+1)T} \overline{\mathbf{k}}^{(k+1)}. \tag{5}$$

Using (4) and (5), we can write

$$d \approx \sqrt{W\left(1 - E\left[\gamma^{(k+1)}\right]\right)}. \tag{6}$$

On initial transient phase in training period of RLS, $E[\gamma^{(k)}]$ starts with very small value, and then it converges to 1 according to the inverse law: $E[\gamma^{(k)}] \approx 1 - ((T-1)/k)$ [16]. Hence, in case of RLSLMS-PTEQ, the large eigenvalue spread of $R_{\mathbf{lu}}$ induced by the small value of $E[\gamma^{(k)}]$ on the initial transient phase causes the convergence rate to be slow. Thus, it can be said that RLS property of RLSLMS-PTEQ is helpful in the steady-state phase but is not too much effective in the initial transition phase.

3. TOL-PTEQ

3.1. Algorithm and Architecture. We show the TOL-PTEQ of which structure is depicted in Figure 3. There is no RLS in TOL-PTEQ. As mentioned in Section 2.2, RLSLMS-PTEQ suffers from slow convergence in its initial transition phase. Two different optimization criteria in one recursive algorithm may work poorly in the initial transition phase. Therefore, decorrelation of $\mathbf{d}^{(k)}$ in TOL-PTEQ is performed by stochastic-gradient algorithm. In general, convergence performance of adaptive algorithm using stochastic-gradient decorrelation method lies in between those of LMS and RLS, which is also applied to TOL-PTEQ as shown in simulation results in Section 3. As TOL-PTEQ operates entirely in a stochastic-gradient criterion, its misadjustment in a steady state is worse than that of RLS-PTEQ. But, as in our simulation results, TOL-PTEQ reach a certain steady-state error level faster than RLSLMS-PTEQ. TOL-PTEQ also inherits lattice features such as easily implemented modular structure, computational efficiency, and numerical stability. Complete algorithm of TOL-PTEQ and complexity analysis is written in the rest of this subsection.

Algorithm: TOL-PTEQ. The algorithm is as follows.

Tone independent:

For $n = 0, 1, \ldots, T-2$

$$f_0^{(k)}(n) = b_0^{(k)}(n) = d_0^{(k)}. \tag{7}$$

For $m = 0, 1, \ldots, \min(n, T-3)$

$$\begin{aligned}
f_{m+1}^{(k)}(n) &= f_m^{(k)}(n) + K_m^{(k)}(n)\, b_m^{(k)}(n-1), \\
b_{m+1}^{(k)}(n) &= b_m^{(k)}(n-1) + K_m^{(k)}(n)\, f_m^{(k)}(n), \\
E_m^{(k)}(n) &= (1-\beta) E_m^{(k)}(n-1) \\
&\quad + \beta\left(f_m^{(k)2}(n) + b_m^{(k)2}(n-1)\right), \\
K_m^{(k)}(n) &= K_m^{(k)}(n-1) + \mu\left(a + E_m^{(k)}(n)\right)^{-1} \\
&\quad \cdot \left(f_m^{(k)}(n)\, b_{m+1}^{(k)}(n) \right. \\
&\quad \left. + b_m^{(k)}(n-1)\, f_{m+1}^{(k)}(n)\right).
\end{aligned} \tag{8}$$

Tone dependent:

$$\begin{aligned}
C_i^{(k)} &= (1-\beta) C_i^{(k)} + \beta \left|Y_i^{(k)}\right|^2, \\
\overline{\mathbf{v}}_i^{(k+1)} &= \overline{\mathbf{v}}_i^{(k)} + \mu \mathbf{c}_i^{(k)} e_i^{(k)*},
\end{aligned} \tag{9}$$

Table 1: Computational complexity for PTEQs.

	Multiplications	Square-root operations	Divisions
TOL-PTEQ	$3T^2 + (4N-2)T + 5$	0	$T-2$
RLS-PTEQ	$3T^2 + (20N+1)T + 10N - 4$	$T + N - 1$	0
RLSLMS-PTEQ	$3T^2 + (4N+1)T + 12N - 4$	$T - 1$	0
NLMS-PTEQ	$(T-1) + (4T+8)N$	0	1

where $f_m^{(k)}(n)$ and $b_m^{(k)}(n)$ are mth-order forward and backward prediction error, $K_m^{(k)}(n)$ is the partial correlation coefficient, $e_i^{(k)} \equiv X_i^{(k)} - \overline{\mathbf{v}}_i^{(k)H}\mathbf{c}_i^{(k)}$, and $\mathbf{c}_i^{(k)} \equiv \left[\mathbf{b}^{(k)T} \;\; Y_i^{(k)}/C_i^{(k)}\right]^T$. Tone-independent part of the algorithm consists of lattice modules, in which the update equations for partial correlation coefficients in (8) are based on gradient adaptive method [17]. Equation (9) in the tone dependent part is the computationally efficient LMS algorithm

The whole algorithm requires $3T^2 + (4N-2)T + 5$ multiplications and $T-2$ divisions. Computation complexities of PTEQs are written in Table 1. RLS-PTEQ and RLSLMS-PTEQ require $3T^2 + (20N+1)T + 10N - 4$ and $3T^2 + (4N+1)T + 12N - 4$ multiplications, respectively. They also require $T + N - 1$ and $T - 1$ square-root operations. Compared with the two PTEQs, TOL-PTEQ reduces $(16N+1)T + 5N - 4$ and $T + 12N + 1$ multipliers, respectively. In the sense that square-root operations and division are performed by Newton's method, it is considered that they require the same order of multiplications. Thus, it can be said that TOL-PTEQ saves $N+1$ multiplications and one square-root operation compared with RLS-PTEQ and RLSLMS-PTEQ, respectively. NLMS-PTEQ has the smallest number of multiplications; however the performance of this algorithm is lower than that of the other algorithms.

3.2. Convergence Analysis. We extend convergence model described in [17] to TOL-PTEQ. Convergence model for TOL-PTEQ consists of three parts; one is the model for forward and backward predictors as described in [17], and the other two parts are the learning-curve models of $E[\overline{\mathbf{v}}_i^{(k)}]$ and $E[|e_i^{(k)}|^2]$ which are written here as follows. Equation (9) can be written as

$$\overline{\mathbf{v}}_i^{(k+1)} = \left(\mathbf{I} - \mu\mathbf{c}_i^{(k)}\mathbf{c}_i^{(k)H}\right)\overline{\mathbf{v}}_i^{(k)} + \mu\mathbf{c}_i^{(k)}X_i^{(k)*}. \tag{10}$$

By taking expectation of both sides of (10), we can write

$$\begin{aligned} E\left[\overline{\mathbf{v}}_i^{(k+1)}\right] &= E\left[\left(\mathbf{I} - \mu\mathbf{c}_i^{(k)}\mathbf{c}_i^{(k)H}\right)\overline{\mathbf{v}}_i^{(k)}\right] + \mu E\left[\mathbf{c}_i^{(k)}X_i^{(k)*}\right] \\ &\approx \left(\mathbf{I} - \mu E\left[\mathbf{c}_i^{(k)}\mathbf{c}_i^{(k)H}\right]\right)E\left[\overline{\mathbf{v}}_i^{(k)}\right] + \mu E\left[\mathbf{c}_i^{(k)}X_i^{(k)*}\right]. \end{aligned} \tag{11}$$

The (m,n)th element of $E[\mathbf{c}_i^{(k)}\mathbf{c}_i^{(k)H}]$ in (11) can be computed as

$$\begin{aligned} E\left[\mathbf{c}_i^{(k)}\mathbf{c}_i^{(k)H}\right]_{(1,1)} &= E\left[|Y_i|^2\right], \\ E\left[\mathbf{c}_i^{(k)}\mathbf{c}_i^{(k)H}\right]_{(1,n\neq 1)} &= E\left[Y_i\left(d_n^{(k)} - \sum_{j=n+1}^{T-2} f_{b,j}^{(k)}d_j^{(k)}\right)\right] \\ &\approx E\left[Y_i d_n^{(k)}\right] - \sum_{j=n+1}^{T-2} f_{b,j}^{(k)}E\left[Y_i d_j^{(k)}\right], \\ E\left[\mathbf{c}_i^{(k)}\mathbf{c}_i^{(k)H}\right]_{(m\neq 1,1)} &= E\left[\mathbf{c}_i^{(k)}\mathbf{c}_i^{(k)H}\right]^*_{(1,n\neq 1)}, \\ E\left[\mathbf{c}_i^{(k)}\mathbf{c}_i^{(k)H}\right]_{(m\neq 1,n\neq 1)} &= E\left[\left(d_m^{(k)} - \sum_{j=m+1}^{T-2} f_{b,j}^{(k)}d_j^{(k)}\right)\left(d_n^{(k)} - \sum_{p=n+1}^{T-2} f_{b,p}^{(k)}d_p^{(k)}\right)\right] \\ &\approx E\left[d_m^{(k)}d_n^{(k)}\right] - \sum_{p=n+1}^{T-2} f_{b,p}^{(k)}E\left[d_m^{(k)}d_p^{(k)}\right] \\ &\quad - \sum_{j=m+1}^{T-2} f_{b,j}^{(k)}E\left[d_j^{(k)}d_n^{(k)}\right] \\ &\quad + \sum_{j=n+1}^{T-2}\sum_{p=n+1}^{T-2} f_{b,j}^{(k)}f_{b,p}^{(k)}E\left[d_j^{(k)}d_p^{(k)}\right], \end{aligned} \tag{12}$$

and mth element of $E[\mathbf{c}_i^{(k)}X_i^{(k)*}]$ can be computed as

$$\begin{aligned} E\left[\mathbf{c}_i^{(k)}X_i^{(k)*}\right]_{m=1} &= E\left[Y_i^{(k)}X_i^{(k)*}\right], \\ E\left[\mathbf{c}_i^{(k)}X_i^{(k)*}\right]_{m\neq 1} &= E\left[\left(d_m^{(k)} - \sum_{j=m+1}^{T-2} f_{b,j}^{(k)}d_j^{(k)}\right)X_i^{(k)*}\right] \\ &\approx E\left[d_m^{(k)}X_i^{(k)*}\right] - \sum_{j=m+1}^{T-2} f_{b,j}^{(k)}E\left[d_j^{(k)}X_i^{(k)*}\right], \end{aligned} \tag{13}$$

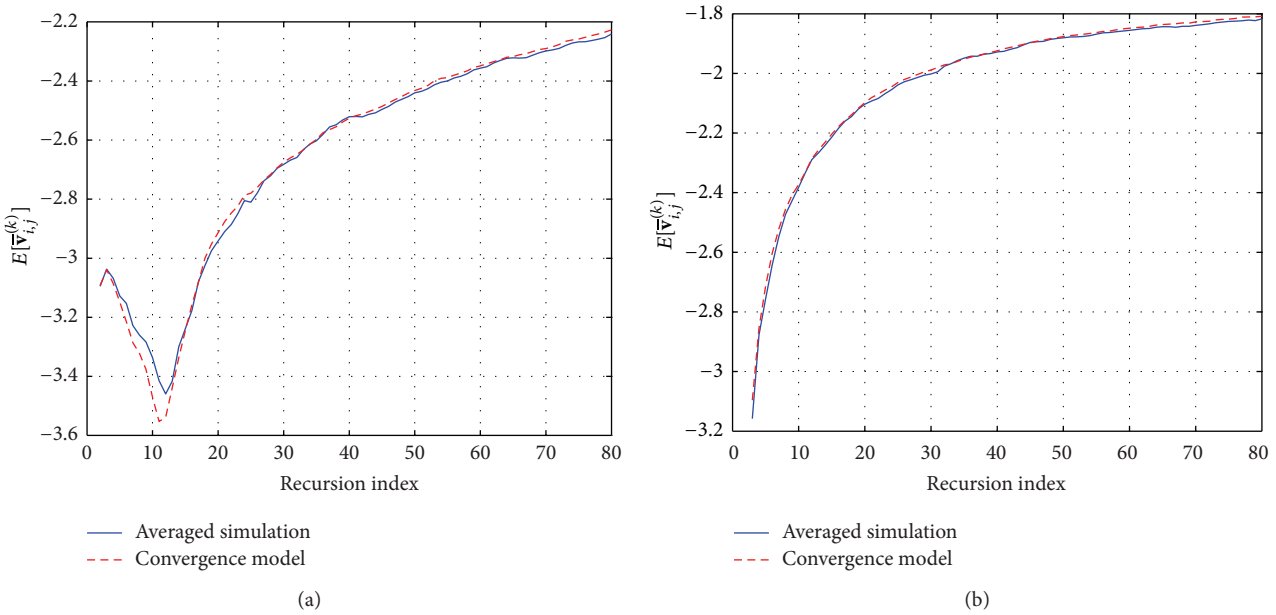

FIGURE 4: Trajectories of $E[\bar{v}_{i,j}^{(k)}]$; dashed line is for convergence model, and solid line is for averaged simulation result. (a) $j = 3$; (b) $j = 12$.

where $m, n \in \{1, 2, \ldots, T-2\}$ and the computation of $E[d_m^{(k)} d_n^{(k)}]$ and $f_{b,m}^{(k)}$ in the above equations are provided in [17]. Mean square error, $E[|e_i^{(k)}|^2]$, can be computed as

$$\begin{aligned}
\text{M.S.E} &= E\left[\left|X_i^{(k)}\right|^2 - \bar{\mathbf{v}}_i^{(k)T} X_i^{(k)} \mathbf{c}_i^{(k)*} \right. \\
&\qquad \left. - \bar{\mathbf{v}}_i^{(k)H} X_i^{(k)} \mathbf{c}_i^{(k)} + \bar{\mathbf{v}}_i^{(k)H} \mathbf{c}_i^{(k)} \mathbf{c}_i^{(k)H} \bar{\mathbf{v}}_i^{(k)}\right] \\
&\approx E\left[\left|X_i^{(k)}\right|^2\right] - \bar{\mathbf{v}}_i^{(k)T} E\left[X_i^{(k)} \mathbf{c}_i^{(k)*}\right] \\
&\quad - \bar{\mathbf{v}}_i^{(k)H} E\left[X_i^{(k)} \mathbf{c}_i^{(k)}\right] + \bar{\mathbf{v}}_i^{(k)H} E\left[\mathbf{c}_i^{(k)} \mathbf{c}_i^{(k)H}\right] \bar{\mathbf{v}}_i^{(k)},
\end{aligned} \tag{14}$$

where $E[X_i^{(k)} \mathbf{c}_i^{(k)}]$ and $E[\mathbf{c}_i^{(k)} \mathbf{c}_i^{(k)H}]$ can be obtained by the same manner as in (11). We obtained two learning curve models as the equalizer tap-weight model (11) and the mean square error model (14).

For example, trajectories of $E[\bar{v}_{i,j}^{(k)}]$ for $j = 3$ and $j = 12$ at $i = 100$ are depicted in Figures 4(a) and 4(b). In the figures, it is also shown that the equalizer tap-weight model (11) coincides with that of simulation results, where simulation results are obtained by averaging over 1000 independent trials. Detailed simulation setup will be seen in the first paragraph of the next section. Figure 5 shows the trajectories of the mean square error, $E[|e_i^{(k)}|^2]$ ($i = 100$). The mean square error (M.S.E) model (14) also accurately tracks the mean square error of the simulation results. From Figure 4, it can be said that the convergence model of TOL-PTEQ is accurate with small β; it is also mentioned in [17] that small β results in accurate convergence model.

Cumulative distribution function of eigenvalues for $\mathbf{u}^{(k)}$ and $\mathbf{c}^{(k)}$ is depicted in Figure 6. This shows that TOL-PTEQ effectively decorrelates $\mathbf{u}^{(k)}$ to $\mathbf{c}^{(k)}$ that helps TOL-PTEQ speed up the convergence.

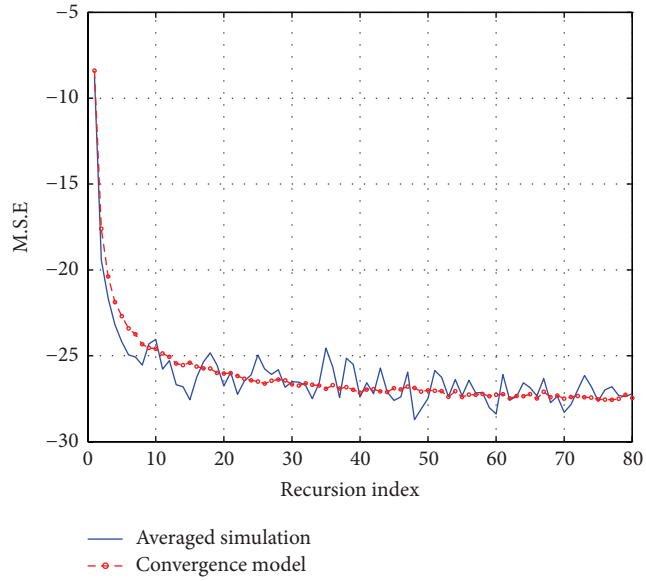

FIGURE 5: M.S.E trajectories with $T = 16$; dashed line is for convergence model, and solid line is for averaged simulation result.

4. Simulation Results

This section provides simulation results of learning curves of four PTEQs and further detailed simulations for analysis of convergence rate according to SNR and order of PTEQ tap weights.

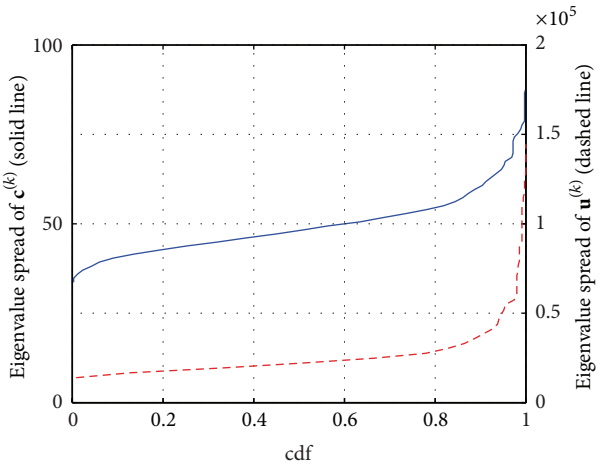

Figure 6: Cumulative distribution function of eigenvalue spread (solid line: $\mathbf{u}^{(k)}$, dashed line: $\mathbf{c}^{(k)}$).

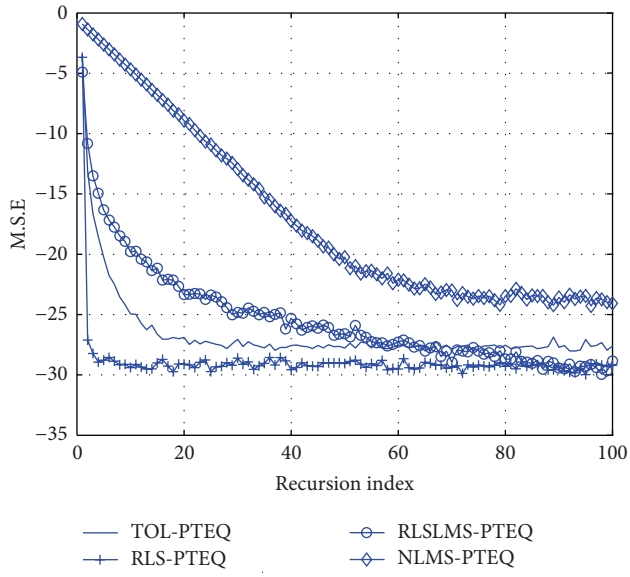

Figure 7: Comparison of M.S.E trajectories for PTEQs.

Maximum scalable OFDMA downlink of mobile WiMAX [18] is considered for this simulation, where signal bandwidth is 20 MHz, the FFT size is 2048, the number of pilot subcarriers is 240, and the number of data subcarriers N_u is 1440. Extended ITU Vehicular A channel model [19] with additive white Gaussian noise is considered. The number of cyclic prefix is set to 64, where it is set to 256 in the standard [18]. This enhances spectral efficiency of about 10 percent compared with the standard in [18].

TOL-PTEQ is compared with NLMS-PTEQ, RLS-PTEQ, and RLSLMS-PTEQ. All simulations are performed over 1000 independent trials. All PTEQs have their order, T, as 16, step-size parameter μ in NLMS part is 1, forgetting factor in RLS part is 0.998, and β of TOL-PTEQ is 0.1.

Learning curves of the four PTEQs are shown in Figure 7. Among the four PTEQs, the convergence rate of RLS-PTEQ

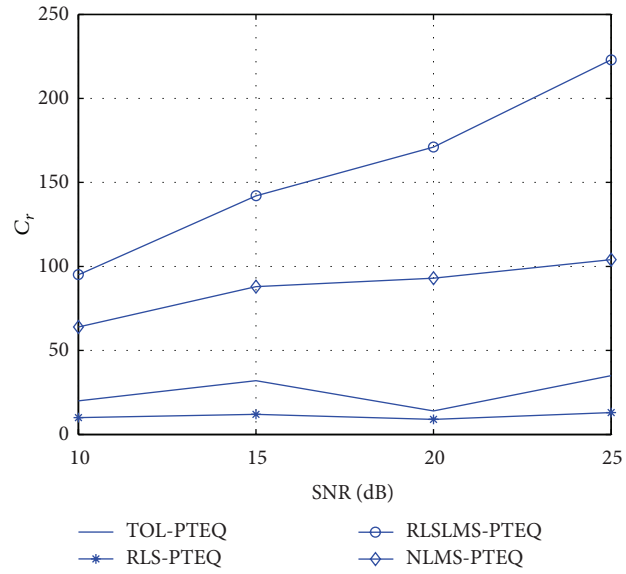

Figure 8: Comparison of C_r versus SNR for PTEQs.

is the fastest and its steady-state M.S.E is the smallest at the expense of the largest computational complexity as described in Section 3.1. NLMS-PTEQ has the smallest computational complexity, but its performance is the worst. RLSLMS-PTEQ converges to the same M.S.E as RLS-PTEQ; however its convergence rate is very slow which is undesirable to the packet-based wireless communications. It can be seen that TOL-PTEQ, in spite of its slightly higher steady-state M.S.E compared with those of the two RLS-typed PTEQs, has very fast convergence rate with the smaller computational complexity than the two RLS-typed PTEQs.

To see the more specific behavior of the convergence, we define the convergence rate C_r as the number of symbols that is required until the M.S.E reaches 98 percent of its steady-state M.S.E. In this analysis, NLMS-PTEQ is excluded because its convergence rate and steady-state M.S.E are of too low performance to be compared with other PTEQs.

Two factors, SNR and order of PTEQ tap-weights, are considered in this simulation analysis. It is desirable that C_r is maintained as small as possible regardless of these factors. Figure 8 shows the C_r depending on SNR, where SNR is ranged from 10 dB to 25 dB. C_r of TOL-PTEQ and RLS-PTEQ are small and independent of the variation of SNR, while C_r of RLSLMS-PTEQ increases as SNR increases. This shows that convergence rate of TOL-PTEQ does not deteriorate at low SNR. In Figure 9, C_r according to the variation of tap-weight order T are shown, where $2 \leq T \leq 30$. It is shown that TOL-PTEQ keeps C_r small with little dependency on T. Hence TOL-PTEQ maintains small values of C_r over simulated SNR and T which is a desirable feature of PTEQ designs.

5. Conclusions and Future Works

We analyzed convergence of several existing PTEQs. Then, we showed the TOL-PTEQ that has enhanced convergence rate with small computational complexity. We also provided

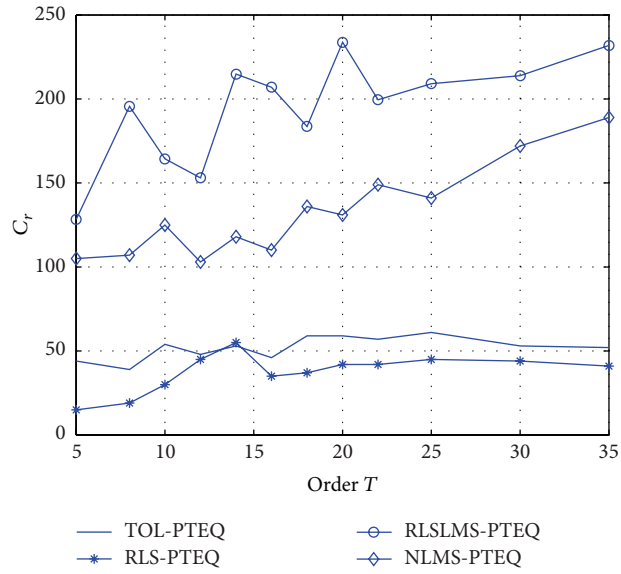

FIGURE 9: Comparison of C_r versus T for PTEQs.

the convergence model of TOL-PTEQ, and it was shown to be accurate by the comparison between the model and simulation results. In the comparison of M.S.E learning curves of the three PTEQs for the mobile WiMAX with the extended ITU Vehicular A channel model, it was shown that TOL-PTEQ has the slower convergence rate than RLS-PTEQ, but its convergence was stabilized within the size of cyclic prefix. It was also shown that TOL-PTEQ had desirable features that its convergence rate was rarely dependent on either SNR or tap-weight order T. TOL-PTEQ can be applied to the radar channel estimation such as long impulse responses with short cyclic prefix. In our future work, we will extend TOL-PTEQ to the multitone based radar systems.

Conflict of Interests

The authors declare that there is no conflict of interests regarding the publication of this paper.

Acknowledgment

This work was supported by MKE/ISDK (Development of Mobile Safety-Inspection Systems Using High Resolution Penetration Imaging Technology for Transportation Infrastructure).

References

[1] K. van Acker, G. Leus, M. Moonen, O. van de Wiel, and T. Pollet, "Per tone equalization for DMT-based systems," *IEEE Transactions on Communications*, vol. 49, no. 1, pp. 109–119, 2001.

[2] K. van Acker, G. Leus, M. Moonen, and T. Pollet, "RLS-based initialization for per-tone equalizers in DMT receivers," *IEEE Transactions on Communications*, vol. 51, no. 6, pp. 885–889, 2003.

[3] S. Sitjongsataporn and P. Yuvapoositanon, "Bit rate maximising per-tone equalisation with adaptive implementation for dmt-based systems," *Eurasip Journal on Advances in Signal Processing*, vol. 2009, Article ID 380560, 2009.

[4] G. Arslan, B. L. Evans, and S. Kiaei, "Equalization for discrete multitone transceivers to maximize bit rate," *IEEE Transactions on Signal Processing*, vol. 49, no. 12, pp. 3123–3135, 2001.

[5] J. Zhang, C.-D. Wu, Y.-Z. Zhang, and P. Ji, "Energy-efficient adaptive dynamic sensor scheduling for target monitoring in wireless sensor networks," *ETRI Journal*, vol. 33, no. 6, pp. 857–863, 2011.

[6] S. -M. Yoo and P. H. Chou, "MHP: Master-Handoff protocol for fast and energy-efficient data transfer over SPI in wireless sensing systems," *ETRI Journal*, vol. 34, no. 4, pp. 553–563, 2012.

[7] Y. Geum, C. Kim, S. Lee, and M.-S Kim, "Technological convergence of IT and BT: evidence from patent analysis," *ETRI Journal*, vol. 34, no. 3, pp. 439–449, 2012.

[8] H. Alemdar and C. Ersoy, "Wireless sensor networks for healthcare: a survey," *Computer Networks*, vol. 54, no. 15, pp. 2688–2710, 2010.

[9] W. Han, A. T. Erdogan, T. Arslan, and M. Hasan, "High-performance low-power FFT cores," *ETRI Journal*, vol. 30, no. 3, pp. 451–460, 2008.

[10] D. K. Kim, Y. W. Choi, and D. W. Kang, "Feasibility study of multi-carrier ground penetrating radar technology," in *Proceedings of the 4th International Conference on Next Generation Information Technologies*, pp. 715–720, June 2013.

[11] D. Kim and G. L. Stüber, "Residual ISI cancellation for OFDM with applications to HDTV broadcasting," *IEEE Journal on Selected Areas in Communications*, vol. 16, no. 8, pp. 1590–1599, 1998.

[12] A. J. Lowery, "Reducing cyclic prefix overhead in optical OFDM systems," in *Proceedings of the 35th European Conference on Optical Communication (ECOC '09)*, Vienna, Austria, September 2009.

[13] N. Al-Dhahir, "Optimum finite-length equalization for multicamer transceivers," *IEEE Transactions on Communications*, vol. 44, no. 1, pp. 56–64, 1996.

[14] R. Baldemair and P. Frenger, "A time-domain equalizer minimizing intersymbol and intercarrier interference in DMT systems," in *Proceedings of the IEEE Global Telecommunicatins Conference (GLOBECOM '01)*, vol. 1, pp. 381–385, San Antonio, Tex, USA, November 2001.

[15] K. van Acker, G. Leus, M. Moonen, and T. Pollet, "RLS-based initialization for per-tone equalizers in DMT receivers," *IEEE Transactions on Communications*, vol. 51, no. 6, pp. 885–889, 2003.

[16] S. Haykin, *Adaptive Filter Theory*, Prentice Hall, 3rd edition, 1996.

[17] M. L. Honig and D. G. Messerschmitt, "Convergence properties of an adaptive digital lattice filter," *IEEE Transactions on Circuits and Systems*, vol. 28, no. 6, pp. 482–493, 1981.

[18] WiMAX Forum, *Mobile WiMAX-Part I: A. Technical Overview and Performance Evaluation*, 2006.

[19] T. B. Sorensen, P. E. Mogensen, and F. Frederiksen, "Extension of the ITU channel models for wideband OFDM systems," in *Proceedings of the 62nd IEEE Vehicular Technology Conference (VTC-Fall '05)*, vol. 1, pp. 392–396, Dallas, Tex, USA, September 2005.